Electrodeposition of Crystalline Si Using a Liquid Zn Electrode in Molten KF-KCl-KSiF

AUTHOR(S):

Moteki, Wataru; Norikawa, Yutaro; Nohira, Toshiyuki

CITATION:

Moteki, Wataru ...[et al]. Electrodeposition of Crystalline Si Using a Liquid Zn Electrode in Molten KF-KCl-KSiF. Journal of The Electrochemical Society 2023, 170(6): 062506.

ISSUE DATE:

2023-06

URL:

http://hdl.handle.net/2433/284727

Journal of The Electrochemical Society

The Electrochemical Society
Advancing solid state & electrochemical science & technology

OPEN ACCESS

Electrodeposition of Crystalline Si Using a Liquid Zn Electrode in Molten KF–KCl–K_2SiF_6

To cite this article: Wataru Moteki *et al* 2023 *J. Electrochem. Soc.* **170** 062506

Journal of The Electrochemical Society, 2023 **170** 062506

Electrodeposition of Crystalline Si Using a Liquid Zn Electrode in Molten KF–KCl–K_2SiF_6

Wataru Moteki, Yutaro Norikawa,* and Toshiyuki Nohira*,z

Energy, Kyoto University, Gokasho, Uji, Kyoto 611-0011, Japan

In this study, we propose a novel Si electrodeposition method using a liquid Zn electrode in molten KF–KCl. Electrochemical measurements and electrolysis were conducted in a KF–KCl–K_2SiF_6 melt at 923 K. Cyclic voltammograms at a liquid Zn electrode revealed that the reduction currents at 0.75–1.0 V vs K^+/K were attributed to the formation of Si–Zn liquid alloy. Additionally, Si was deposited through potentiostatic electrolysis at 0.75 V using liquid Zn in a boron nitride (BN) crucible as an electrode. Cross-sectional scanning electron microscopy and energy-dispersive X-ray spectroscopy showed that deposited Si was located at the bottom and side of the interface between Zn and the BN crucible instead of at the interface between Zn and the molten salt, indicating the electrodeposition of Si attributed to Si–Zn liquid alloy formation. The obtained Si was confirmed to be the crystalline form by X-ray diffractometry, and the maximum grain size was approximately 2 mm. Galvanostatic electrolysis at –20 mA cm^{-2} with varying electrical charges showed that the Si grain size increased with increasing charge, confirming the growth of crystalline Si. Finally, the mechanism of Si electrodeposition on a Zn electrode through Si–Zn alloying was discussed.
 [DOI: 10.1149/1945-7111/acd9ef]

Manuscript submitted March 22, 2023; revised manuscript received May 11, 2023. Published June 14, 2023. *This paper is part of the JES Focus Issue on Molten Salts and Ionic Liquids III.*

Crystalline Si solar cells account for 97% of all solar cell production owing to their high efficiency and durability.[1] Since the 2000s, the production of crystalline Si solar cells has been increasing yearly.[1] High-purity polycrystalline Si for crystalline Si solar cell substrates is produced using the Siemens process, a chemical vapor deposition method that employs trichlorosilane. The Si ingot obtained from this method is sliced into the substrate form. However, this process has some limitations, such as high energy costs and low yield owing to kerf loss. To address these limitations, researchers have proposed electrodeposition methods that facilitate direct crystalline Si film deposition on the substrates, resulting in lower production costs.[2]

The electrodeposition method can form films at high speed and on complicated shapes. Si electrodeposition using high-temperature molten salts yields highly crystalline Si.[2] Several studies have demonstrated Si electrodeposition using fluoride,[3–11] chloride,[12–19] and fluoride–chloride mixed molten salts.[20–30] We focused on using the KF–KCl molten salt because of the following advantages. First, the high fluoride ion concentration enables SiF_6^{2-} ions to exist stably in the melt.[2] Second, both KF and KCl have high solubilities in water,[31] so the salt adhering to the surface of the electrodeposited material can be easily removed. Third, since the anode reaction can be set to generate Cl_2, closed-cycle operation is possible when $SiCl_4$ is introduced as the Si source.[28] And so far, we have reported Si electrodeposition using the KF–KCl mixed molten salt as an electrolyte and K_2SiF_6 or $SiCl_4$ as a Si source.[26–30] Purity levels of the deposited Si film of up to 4 N or higher have been achieved, and the semiconductor properties of the deposited Si film have been confirmed through photoelectrochemical measurements.[30] The effect of bath temperature on crystallite size was investigated in this molten salt system revealing that the crystallite size increased with increasing bath temperature.[29] However, the crystal grain size in the Si electrodeposition method described above is not sufficiently large. Smaller crystalline particles have more grain boundaries, which can reduce conversion efficiency by promoting electron–hole recombination generated by light at the grain boundaries. Therefore, obtaining highly pure Si with large grain size is necessary. In a previous report, the size of Si crystal particles at 923 K was calculated to be 50 nm, and the maximum size observed at 1073 K was only 20 μm.[29]

Liquid metal electrodes may provide a solution for increasing the grain size of Si. According to previous studies on Si deposition using organic solvents and room temperature ionic liquids, crystalline Si can be electrodeposited using liquid Ga electrodes,[32–35] despite the well-known tendency of amorphous Si electrodeposition on solid electrodes. The mechanism of crystalline Si electrodeposition using liquid metal electrodes involves the reduction of the Si source at the surface of the liquid Ga electrode, followed by the simultaneous dissolution of the reduced Si into the liquid Ga electrode (Si–Ga liquid alloy formation), with continued reduction of the Si source at the surface.[32–35] When the Si concentration in the liquid Ga electrode becomes supersaturated, Si(*s*) and Ga(*l*) are separated,[32–35] promoting crystal growth by forming a liquid metal alloy. These results suggest that using liquid metal electrodes in high-temperature molten salt can produce crystalline Si grains of larger size. While an initial investigation of Si deposition using a liquid Ga electrode in KF–KCl–K_2SiF_6 melt at 923 K has been conducted,[36] further studies are needed to investigate this approach.

This study used Zn as the liquid metal for Si deposition in a high-temperature molten salt for three reasons. First, Zn does not form intermetallic compounds with Si.[37] Second, residual Zn can be easily removed by vacuum evaporation. Third, many impurity elements have small distribution coefficients between solid Si and liquid Zn, making it difficult for impurity elements to contaminate the solid Si.[38]

Electrodeposition of Si with larger grain size was performed using a liquid Zn electrode in a KF–KCl–K_2SiF_6 melt at 923 K. First, cyclic voltammetry measurements were conducted to observe the electrochemical behavior of Si(IV) ions on a liquid Zn electrode. Second, potentiostatic electrolysis was performed to electrodeposit Si via Si–Zn alloying. Third, galvanostatic electrolysis at –20 mA cm^{-2} was conducted to observe the growth of Si crystals by varying the charge on the electrode. Finally, the mechanism of Si deposition was determined.

Experimental

Figure 1a shows the schematic illustration of the experimental apparatus. Reagent grade KF (FUJIFILM Wako Pure Chemical Corp., purity > 99.0%) and KCl (FUJIFILM Wako Pure Chemical Corp., purity > 99.5%) were mixed in a eutectic composition (KF:

*Electrochemical Society Active Member
zE-mail: nohira.toshiyuki.8r@kyoto-u.ac.jp

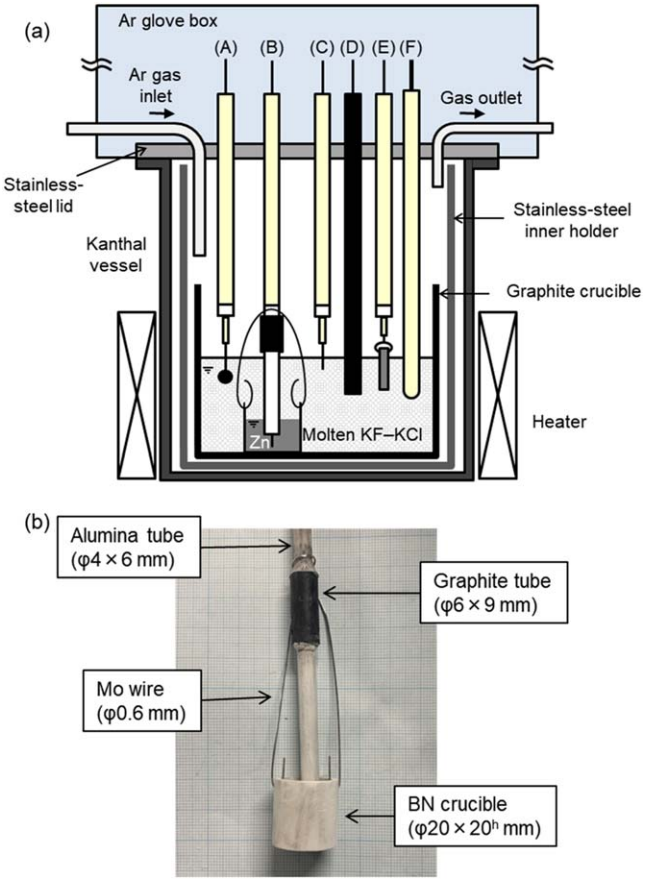

Figure 1. (a) Schematic illustration of the entire experimental apparatus. (A) Ag flag electrode, (B) liquid Zn electrode, (C) Pt wire electrode, (D) carbon rod electrode, (E) Si rod electrode, and (F) thermocouple. (b) Photograph of the liquid Zn electrode.

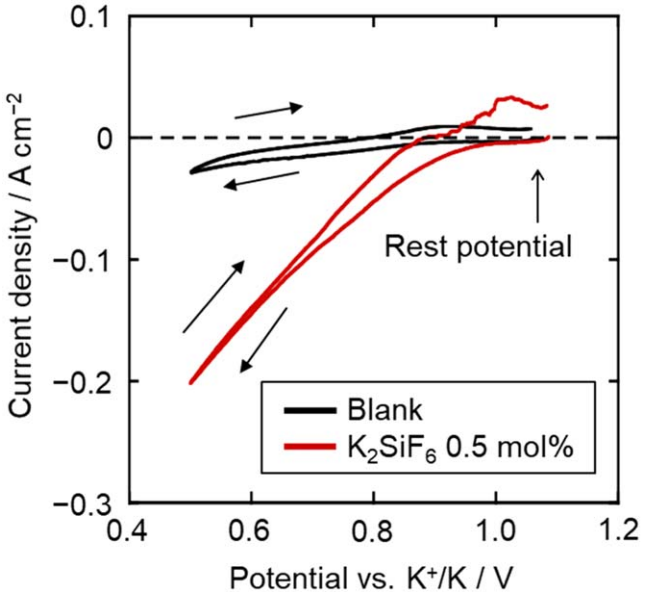

Figure 2. Cyclic voltammograms at a liquid Zn electrode in molten KF–KCl at 923 K before and after adding K_2SiF_6 (0.5 mol%). Scan rate: 0.20 V s^{-1}.

KCl = 45:55 mol%, melting point = 873 K, weight = 400–500 g) and loaded into a graphite crucible (SANKO Co., Ltd., IG-110 grade, o.d. 100 mm × i.d. 90 mm × height 120 mm). The mixture in

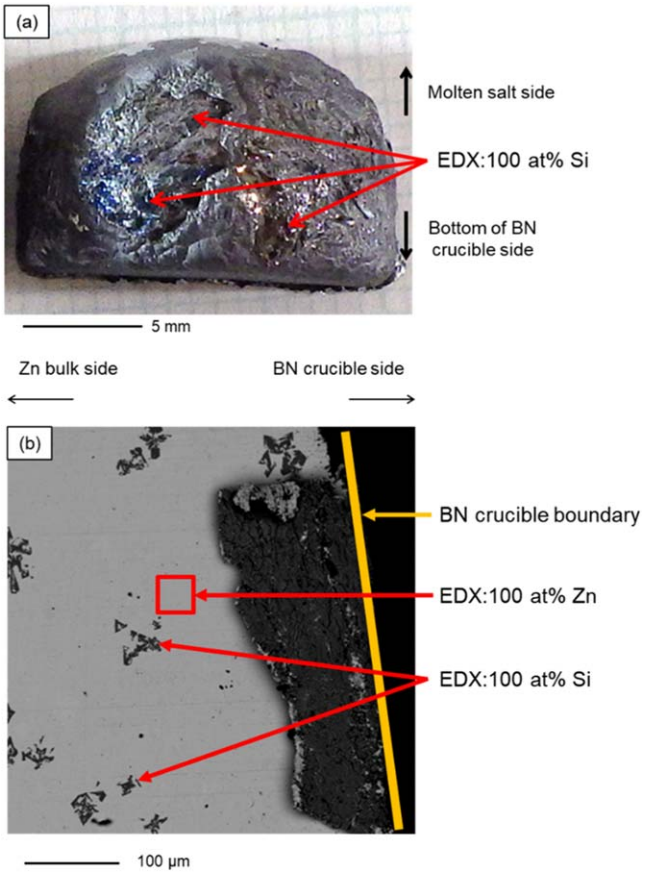

Figure 3. (a) Photograph and (b) cross-sectional SEM image of the Zn electrode sample obtained from potentiostatic electrolysis at 0.75 V for 48 h in molten KF–KCl–K_2SiF_6 (2.0 mol%) at 923 K. Charge: –3312 C.

the crucible was dried under vacuum at 453 K for 72 h and 773 K for 24 h. The mixture in the crucible was placed at the bottom of a stainless-steel vessel in an airtight Kanthal container. Electrochemical measurements were performed at 923 K in a glove box (Yamato, Co., Ltd., pure box system with an electric furnace, ZYS 16–0057) with an Ar atmosphere at conditions of O_2 and H_2O below 1 ppm. After blank measurements in KF–KCl, K_2SiF_6 (Junsei Chemical Co., Ltd., purity > 99.0%) was added to the melt to obtain a concentration of 0.5 or 2.0 mol%.

Electrochemical measurements and galvanostatic electrolysis were performed using the three-electrode method with an electrochemical measurement system (Hokuto Denko Corp., HZ-7000). The working electrodes were liquid Zn (Kojundo Chemical Lab. Co., Ltd., 7 or 13 g, purity = 99.99%) held in a small boron nitride (BN) crucible (Fig. 1b) and an Ag flag (Nilaco Corp., thickness = 0.1 mm, diameter = 3 mm, purity > 99%). The electrochemical continuity of Zn was achieved using a W wire (Nilaco Corp., diameter = 1.0 mm, purity = 99.98%). The structure of the Ag flag electrode is described in detail in a previous study.[26] Si (Furuichi Chemical Corp., diameter = 73 mm, purity = 10 N) or carbon rods (SANKO Co., Ltd., diameter 7 mm × length 520 mm) were used as counter electrodes. A platinum wire (Nilaco Corp, diameter = 1 mm, purity > 99.98%) was used as a quasi-reference electrode for blank measurements, and Si rods were used as the reference electrodes after adding K_2SiF_6. The potential of the reference electrode was calibrated with respect to the K^+/K potential estimated using cyclic voltammetry on a Ag wire (Nilaco Corp., diameter = 1 mm, purity = 99.99%).

After electrolysis, the Zn electrodes were immediately removed from the furnace and cooled in a glove box. Before the solidification of liquid Zn, the Mo wire hanging on the BN crucible was cut, and

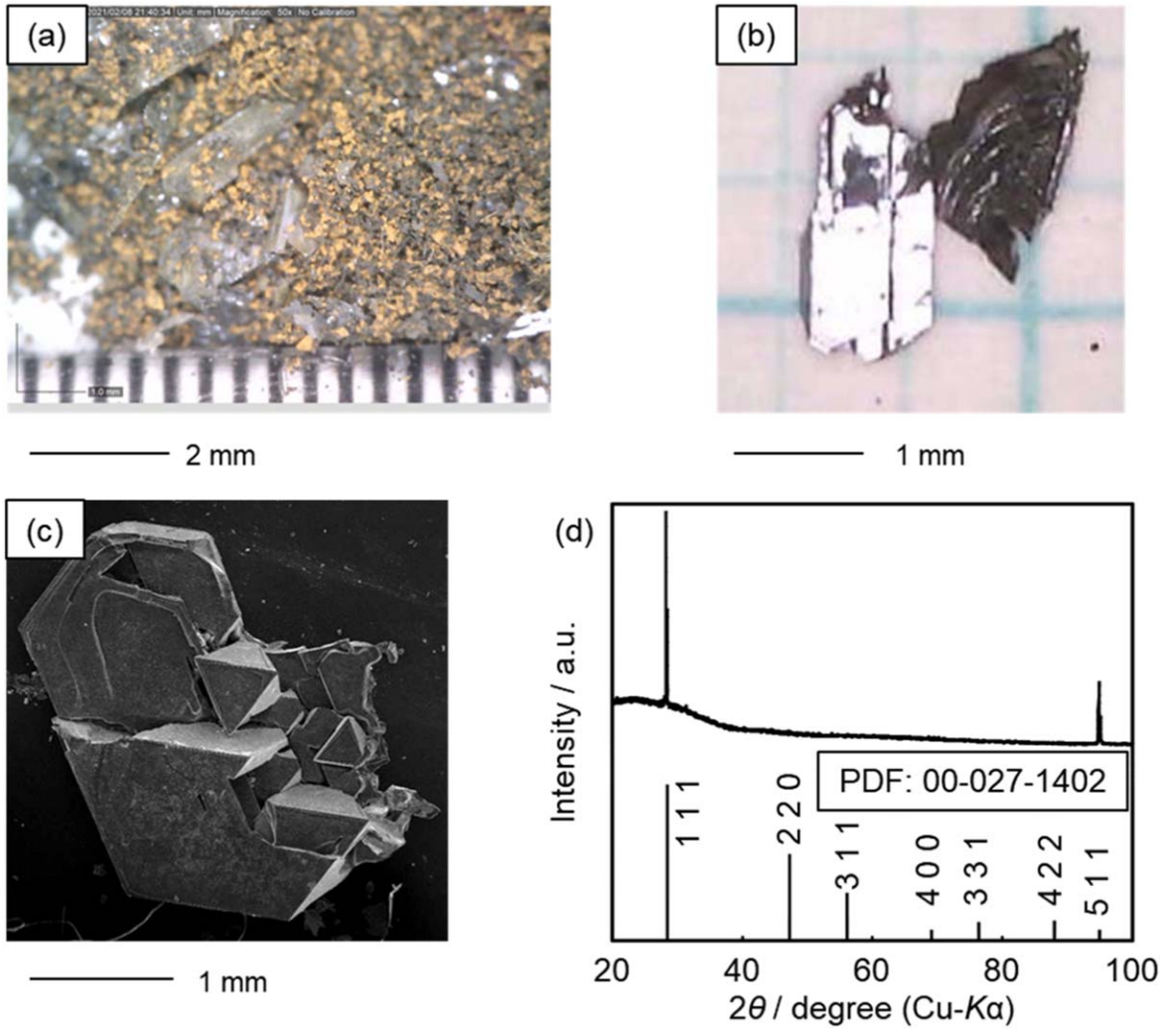

Figure 4. (a) Photograph of deposited Si obtained by potentiostatic electrolysis at 0.75 V for 48 h in molten KF–KCl–K_2SiF_6 (2.0 mol%) at 923 K. (b) Optical microscopy and (c) SEM images of a separated large Si grain. (d) XRD pattern of the separated large Si grain after lightly crushing in a mortar.

the lead wire and BN protection tube were removed from liquid Zn. The small BN crucible was exposed to stirred water to dissolve and eliminate the solidified salt at room temperature. Subsequently, the Zn samples were collected from the bottom of the crucible and further immersed and washed in distilled water at room temperature for 2 h to eliminate the adhered salts.

The samples were characterized using energy-dispersive X-ray spectroscopy (EDX; Thermo Fisher Scientific Inc., SE1200–8001) and X-ray diffraction (XRD; Rigaku Corp., Ultima IV, Cu-Kα line) analyses. The surface of the samples was analyzed using optical microscopy (Sanko, DinoLite Premier S). The surface and cross-section of the samples were analyzed using scanning electron microscopy (SEM; Keyence Corp., VE-8800 or Thermo Fisher Scientific Inc., Phenom Pro Generation 5). The Zn metal lumps were dissolved in 500 ml of HCl solution (20 wt%) to recover the deposited Si granules. After being filtered off, the resulting deposited Si was collected separately based on the grain size using a stainless-steel sieve (AS ONE Corp., sieve opening = 0.1 mm, 0.212 mm, 0.5 mm, and 1 mm). The particle size distribution was examined from the weight of the deposited Si in each particle size range.

Results and Discussion

Reduction behavior of Si(IV) ions using cyclic voltammetry.— First, cyclic voltammetry was performed to investigate the reduction of Si(IV) ions, and the resulting cyclic voltammograms at the liquid Zn electrode in molten KF–KCl before and after the addition of K_2SiF_6 (0.5 mol%) at 923 K are shown in Fig. 2. Before adding K_2SiF_6, a rise in reduction current was observed at approximately 0.8 V, which was attributed to the formation of the liquid K–Zn alloy that exists at 923 K.[39]

$$K^+ + Zn(l) + e^- \rightarrow K - Zn(l) \quad [1]$$

After adding K_2SiF_6, a rise in reduction current, which was not present before, was observed at approximately 1.0 V. The reduction current continued to increase, and at 0.75 V, its value reached about six times larger than before the addition. In our previous work in the same condition, the electrochemical behavior of Si(IV) on solid Ag electrode has been studied, in which the electrodeposition of solid Si occurs at potentials more negative than 0.75 V.[26] Since only Si–Zn liquid alloy exists in the Si–Zn phase diagram at 923 K,[37] the reduction currents at 0.75–1.0 V were attributed to the formation of the Si–Zn liquid alloy.

$$SiF_6^{2-} + Zn(l) + 4e^- \rightarrow Si - Zn(l) + 6F^- \quad [2]$$

Deposition of Si using potentiostatic electrolysis.— To confirm the electrodeposition of Si via the formation of Si–Zn alloy, potentiostatic electrolysis using a liquid Zn electrode was conducted at 0.75 V for 48 h in molten KF–KCl–K_2SiF_6 (2.0 mol%). The

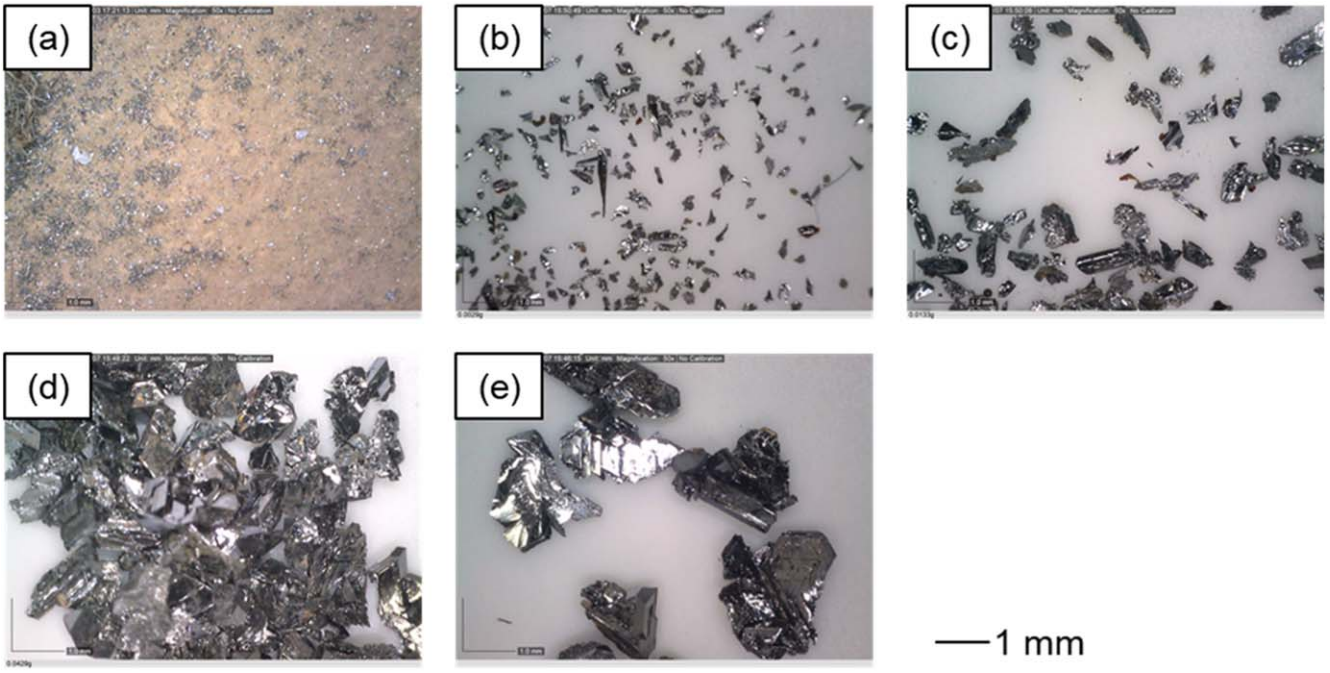

Figure 5. Photographs of Si obtained through galvanostatic electrolysis of a liquid Zn electrode at –20 mA cm^{-2} in molten KF–KCl–K_2SiF_6 (2.0 mol%) at 923 K. Charge on the electrode: –2087 C. The particle sizes of Si are (a) <0.1 mm, (b) 0.1–0.212 mm, (c) 0.212–0.5 mm, (d) 0.5–1 mm, and (e) >1 mm.

charge on the electrode was –3312 C. Theoretically, reducing Si(IV) ions using all the charge on the electrode could form a liquid Si–Zn alloy with 4.3 at% Si. However, per the phase diagram, the solubility of Si is 1 at% at 923 K,[37] suggesting that Si was saturated during the electrolysis.

Figure 3a shows a surface photograph of the Zn electrode removed from the BN small crucible. Large grains with metallic luster were observed at the boundary of the BN crucible and not of the molten salt. EDX analysis of these grains revealed that those large grains were 100 at% Si, indicating Si deposits on the boundary of the BN crucible and not of the molten salt. The Si deposits would have been observed at the boundary of the molten salt only if the solid Si was directly electrodeposited on the liquid Zn electrode. These results confirm that Si was electrodeposited via Si–Zn alloying inside the liquid Zn electrode.

The site on the Zn electrode where Si was deposited via liquid Si–Zn alloying was investigated in detail by analyzing the cross section of the Zn electrode using SEM. As shown in Fig. 3b, small Si particles were detected inside the Zn electrode, suggesting that Si in the Si–Zn alloy on the surface of the Zn electrode diffused into the interior of the electrode. A Si grain of size 200 μm was detected at the interface between the Zn electrode and BN crucible, indicating preferential deposition of Si at the BN crucible boundary. Figures 4a, 4b, and 4c show the photographs and SEM images of Si deposits after hydrochloric acid treatment of the sample. The photograph in Fig. 4a shows varying sizes of the deposited Si, some of which were in the powder form. The photograph and the SEM image in Figs. 4b and 4c of a large Si grain separated from Zn reveal the maximum size of the deposited Si to be approximately 2 mm. This size was much larger than 50 nm, the crystal size of Si obtained on solid electrodes in KF–KCl– K_2SiF_6 melt at 923 K.[29] Figure 4d shows an XRD pattern of the separated large Si, which was lightly crushed in a mortar. The sharp peaks corresponding to the 111 and 511 diffraction peaks of Si were observed, confirming the crystalline form of the electrodeposited Si. The absence of other diffraction peaks was assumed owing to the preferential orientations.

Herein, the deposition mechanism of crystalline Si is discussed in terms of crystal size. Previous reports on Si precipitation showed that decreasing the temperature of liquid Si–Zn alloys decreases the size of the precipitated Si grains at a higher cooling rate.[38] Even at the temperature-decreasing rate of 20 K h^{-1}, only Si grains smaller than 1 mm were obtained.[38] In the present study, the Si–Zn liquid alloy was cooled through natural cooling, and the temperature-decreasing rate was extremely high (approximately 230 K s^{-1}). Therefore, Si powders with small grain sizes could have been deposited during natural cooling.

Crystal growth of deposited Si by increasing electrolysis charge.—To investigate the Si crystal growth during galvanostatic electrolysis, the amount of Si supplied to the liquid Zn electrode was varied by varying the charge on the electrode from –417 C (corresponding to the Si saturation of the Zn electrode) to –4173 C (corresponding to ten times the Si saturation of the Zn electrode) at a current density of –20 mA cm^{-2}. The obtained samples were treated with hydrochloric acid to dissolve Zn. The grains of the deposited Si were separated based on the grain size using sieves. Figures 5a to 5e show photographs of Si grains of varying grain sizes ranging from less than 0.1 mm to more than 1 mm. As seen in the photographs, all Si grains exhibited a metallic luster.

Figures 6a to 6e show the particle size distributions of Si deposited through galvanostatic electrolysis at different charges ranging from –417 to –4173 C. When the amount of charge corresponded to the Si saturation (–417 C, Fig. 6a), the weight ratio of Si grains larger than 0.5 mm was very small, less than 5%. The weight ratio of Si grains larger than 0.5 mm increased with increasing the charge, and Si grains larger than 1 mm were also observed at higher amounts of charges.

The weight ratio of Si larger than 1 mm was maximum when the amount of charge was –4173 C and accounted for over 80% of the Si obtained from the sample. Furthermore, the weight ratio of Si grains smaller than 0.5 mm decreased with increasing charge. These results suggest that the growth of Si grains proceeds with increasing charge. Note that the current efficiency was 80.0% at –4173 C.

Mechanism of electrodeposition of crystalline Si via Si–Zn alloying.—Figure 7 shows a schematic illustration of the proposed process of crystalline Si deposition through electrolysis using a liquid Zn electrode. First, as shown in Fig. 7a, Si(IV) ions are electrochemically reduced to Si at the surface of the liquid Zn electrode, followed by Si–Zn alloy formation by the reduced Si. As

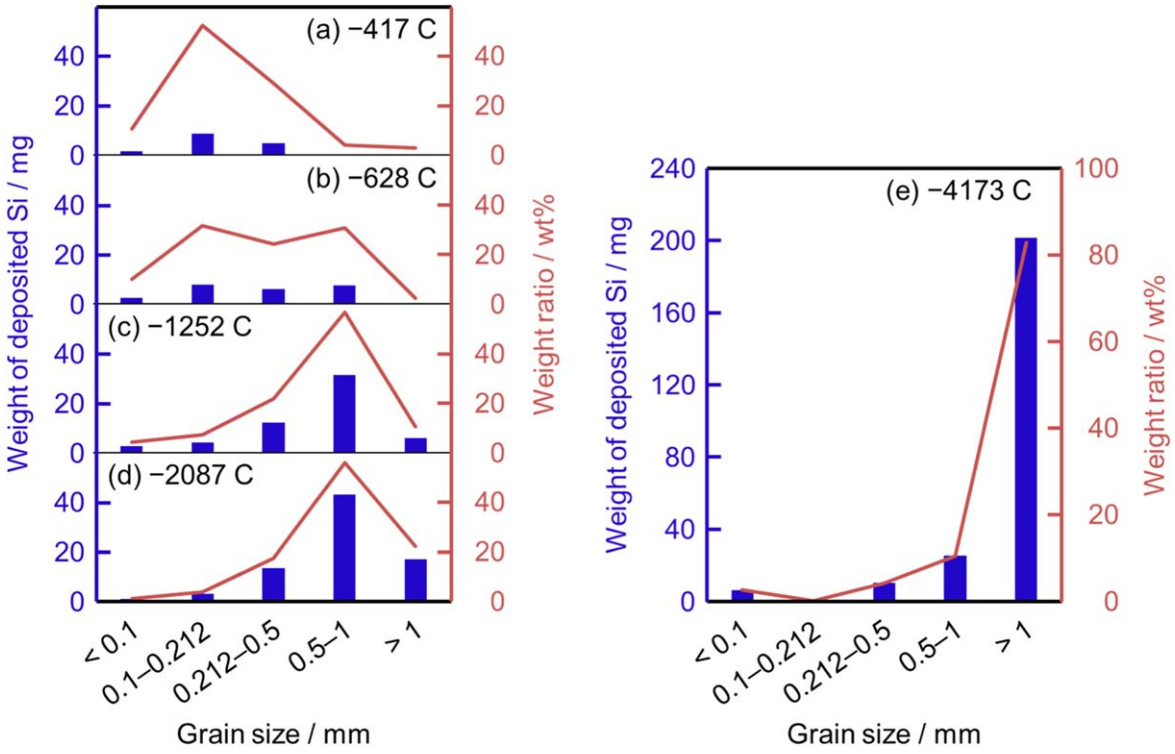

Figure 6. Particle size distributions of the deposited Si obtained via galvanostatic electrolysis at charges of (a) –417 C, (b) –628 C, (c) –1252 C, (d) –2087 C, and (e) –4173 C.

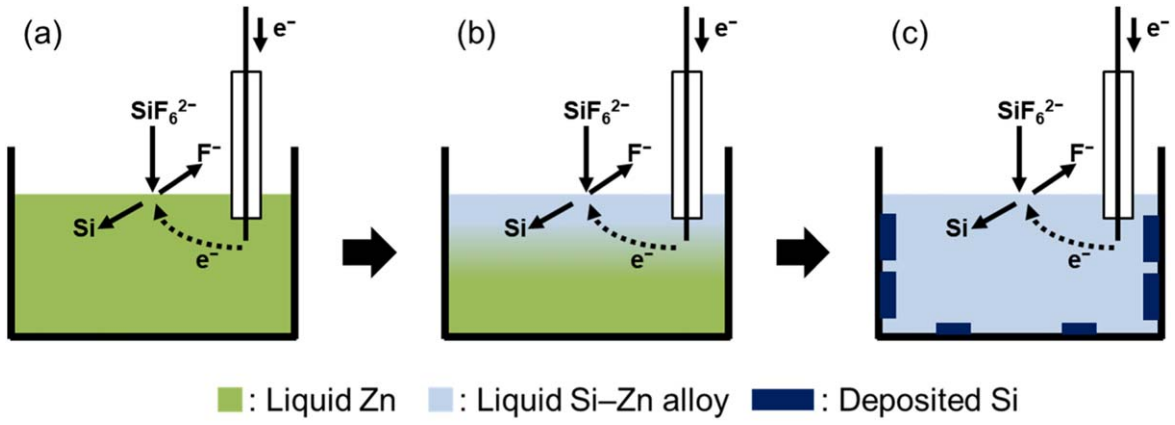

Figure 7. Schematic illustration of crystalline Si deposition through electrolysis using a liquid Zn electrode.

the electrolysis proceeds (Fig. 7b), the Si concentration on the surface of the Zn electrode increases, and Si begins to diffuse on the surface of the electrode. As the charge increases and the Si concentration in the liquid Zn electrode saturates, solid Si deposits inside the liquid Zn electrode. As shown in Fig. 3, crystalline Si is deposited preferentially at the interface between liquid Zn and the BN crucible (Fig. 7c). As discussed earlier, the crystallite size increases with the increasing charge on the electrode. This suggests that almost no new nucleation occurred, and the existing crystallites continued to grow. Thus, electrodepositing Si using a liquid Zn electrode can produce crystalline Si with a larger grain size than conventional electrodeposition using a solid electrode.

Conclusions

Crystalline Si was electrodeposited using a liquid Zn electrode in a KF–KCl–K_2SiF_6 melt at 923 K. Cyclic voltammetry showed that Si(IV) ions reduced to form a liquid Si–Zn alloy, which did not occur when using a solid electrode. In potentiostatic electrolysis at 0.75 V vs K^+/K, crystalline Si with a maximum grain size of approximately 2 mm was deposited inside the liquid Zn electrode. Large Si grains were obtained via the formation of Si–Zn liquid alloy. In galvanostatic electrolysis at –20 mA cm^{-2}, increasing the charge resulted in the deposition of crystalline Si with a larger grain size. Moreover, the weight ratio of Si grains larger than 1 mm was over 80%, with a maximum of –4173 C. The mechanism of Si deposition on a liquid Zn electrode was described in three steps: the formation of Si–Zn liquid alloy at the surface of the Zn electrode, the increase of Si concentration in the Zn electrode, and the deposition of solid Si inside the Zn electrode. By this mechanism, the electrodeposition of Si using a liquid Zn electrode can produce crystalline Si with a larger grain size than conventional electrodeposition using a solid electrode.

Acknowledgments

This study was supported by Grant-in-Aid for Scientific Research A, Grant Number 21H04620, from the Japan Society for the Promotion of Science (JSPS). This study was partly supported by JST, the establishment of university fellowships toward the creation of science technology innovation, Grant Number JPMJFS2123.

ORCID

Wataru Moteki https://orcid.org/0000-0003-2657-9519
Yutaro Norikawa https://orcid.org/0000-0002-0861-5443
Toshiyuki Nohira https://orcid.org/0000-0002-4053-554X

References

1. Photovoltaic Market 2021, (RTS Corp, Tokyo, Japan) (2021), [Japanese].
2. K. Yasuda and T. Nohira, *High. Temp. Mater. Proc.*, **41**, 247 (2022).
3. U. Cohen and R. A. Huggins, *J. Electrochem. Soc.*, **123**, 381 (1976).
4. G. M. Rao, D. Elwell, and R. S. Feigelson, *J. Electrochem. Soc.*, **127**, 1940 (1980).
5. D. Elwell and R. S. Feigelson, *Sol. Energy, Mat.*, **6**, 123 (1982).
6. K. S. Osen, A. M. Martinez, S. Rolseth, H. Gudbrandsen, M. Juel, and G. M. Haarberg, *ECS Trans.*, **33**, 429 (2010).
7. A. L. Bieber, L. Massot, M. Gibilaro, L. Cassayre, P. Taxil, and P. Chamelot, *Electrochim. Acta*, **62**, 282 (2012).
8. G. M. Haarberg, L. Famiyeh, A. M. Martinez, and K. S. Osen, *Electrochim. Acta*, **100**, 226 (2013).
9. Y. Hu, X. Wang, J. Xiao, J. Hou, S. Jiao, and H. Zhu, *J. Electrochem. Soc.*, **160**, D81 (2013).
10. Y. Sakanaka and T. Goto, *Electrochim. Acta*, **164**, 139 (2015).
11. Y. Suzuki, Y. Inoue, M. Yokota, and T. Goto, *J. Electrochem. Soc.*, **166**, D564 (2019).
12. R. Boen and J. Bouteillon, *J. App. Electrochem.*, **13**, 277 (1983).
13. T. Matsuda, S. Nakamura, K. Ide, K. Nyudo, S. Yae, and Y. Nakato, *Chem. Lett.*, **7**, 569 (1996).
14. S. V. Devyatkin, *J. Min. Metall. Sect. B.*, **39**, 303 (2003).
15. J. Zhao, H. Yin, T. Lim, H. Xie, H. Hsu, F. Forouzan, and A. J. Bard, *J. Electrochem. Soc.*, **163**, 506 (2016).
16. Y. Sakanaka, A. Murata, T. Goto, and K. Hachiya, *J. Alloy. Compd.*, **695**, 2131 (2017).
17. X. Yang, L. Ji, X. Zou, T. Lim, J. Zhao, E. T. Yu, and A. J. Bard, *Angew. Chem. Int. Ed.*, **56**, 15078 (2017).
18. X. Zou, L. Ji, X. Yang, T. Lim, E. T. Yu, and A. J. Bard, *J. Am. Chem. Soc.*, **139**, 16060 (2017).
19. Y. Zhang, Y. Zhang, X. Li, J. Liu, M. Zhang, X. Yang, M. Huang, M. Xu, P. Dong, and Z. Zhou, *JOM*, **72**, 2245 (2020).
20. A. A. Andriiko, E. V. Panov, O. I. Boiko, B. V. Yakovlev, and O. Y. Borovik, *Russ. J. Electrochem.*, **33**, 1343 (1997).
21. S. V. Kuznetsova, V. S. Dolmatov, and S. A. Kuznestov, *Russ. J. Electrochem.*, **45**, 797 (2009).
22. Y. P. Zaykov, S. I. Zhuk, A. V. Isakov, O. V. Grishenkova, and V. A. Isaev, *J. Solid State Electrochem.*, **19**, 1341 (2015).
23. J. Peng, H. Yin, J. Zhao, X. Yang, A. J. Bard, and D. R. Sadoway, *Adv. Funct. Mater.*, **28**, 1703551 (2017).
24. S. Zhuk, V. Isaev, O. Grishenkova, A. Isakov, A. Apisarov, and Y. Zaykov, *J. Serb. Chem. Soc.*, **82**, 51 (2017).
25. S. I. Zhuk, A. V. Isakov, A. P. Apisarov, O. V. Grishenkova, V. A. Isaev, E. G. Vovkotrub, and Y. P. Zaykov, *J. Electrochem. Soc.*, **164**, 5135 (2017).
26. K. Maeda, K. Yasuda, T. Nohira, R. Hagiwara, and T. Homma, *J. Electrochem. Soc.*, **162**, D444 (2015).
27. K. Yasuda, K. Maeda, T. Nohira, R. Hagiwara, and T. Homma, *J. Electrochem. Soc.*, **163**, D95 (2016).
28. K. Yasuda, K. Maeda, R. Hagiwara, T. Homma, and T. Nohira, *J. Electrochem. Soc.*, **164**, D67 (2017).
29. K. Yasuda, K. Saeki, T. Kato, R. Hagiwara, and T. Nohira, *J. Electrochem. Soc.*, **165**, D825 (2018).
30. K. Yasuda, T. Kato, Y. Norikawa, and T. Nohira, *J. Electrochem. Soc.*, **168**, 112502 (2021).
31. J. R. Rumble, *CRC Handbook of Chemistry and Physics* (Boca Raton)(CRC Press) 99th ed. (2018).
32. J. Gu, E. Fahrenkrug, and S. Maldonado, *J. Am. Chem. Soc.*, **135**, 1684 (2013).
33. E. Fahrenkrug and S. Maldonado, *Acc. Chem. Res.*, **48**, 1881 (2015).
34. L. Ma, S. Lee, J. DeMuth, and S. Maldonado, *RSC Adv.*, **6**, 78818 (2016).
35. J. Zhang, S. Chen, H. Zhang, S. Zhang, X. Yao, and Z. Shi, *RSC Adv.*, **6**, 12061 (2016).
36. G. M. Haarberg, T. Kato, Y. Norikawa, and T. Nohira, *ECS Trans.*, **89**, 29 (2019).
37. R. W. Olesinski and G. J. Abbaschian, *Bull. Alloy Phase Diagrams*, **6**, 545 (1985).
38. Y. Ma, K. Yasuda, A. Ido, T. Shimao, M. Zhong, R. Hagiwara, and T. Nohira, *Mater. Trans.*, **62**, 403 (2021).
39. A. D. Pelton, *Bull. Alloy Phase Diagrams*, **8**, 548 (1987).